Interdisciplinary Research in Medical Sciences Specialty
ISSN: 3062-4401
2023, Volume 3, Issue 2, Page No: 128-138

Available online at: www.galaxypub.co/page/journals

Galaxy Publication

Radiomic Signatures from Multiparametric MRI to Distinguish TCM Deficiency and Excess Syndromes in Prostate Cancer

Khaled Mansour[1], Omar Haddad[1], Rami Saleh[1]*

[1]Department of Health Informatics, Faculty of Medicine, University of Sharjah, Sharjah, United Arab Emirates.

***E-mail** ✉ rami.saleh.med@gmail.com

Received: 14 May 2023; **Revised:** 05 October 2023; **Accepted:** 07 October 2023

ABSTRACT

This study investigated whether MR-based radiomics can provide imaging biomarkers capable of distinguishing deficiency-type and excess-type Traditional Chinese Medicine (TCM) syndromes in patients with prostate cancer (PCa). A cohort of 121 men with PCa from two institutions was analyzed, with 84 allocated to a training set and 37 to an external validation set. According to TCM diagnostic criteria, patients were classified into deficiency or excess syndrome groups. Quantitative radiomic features were extracted from T2-weighted images (T2WI), diffusion-weighted sequences, and corresponding apparent diffusion coefficient (ADC) maps. Feature selection was performed in the training set using minimum redundancy maximum relevance followed by least absolute shrinkage and selection operator, yielding a radiomic signature for classification. Model performance was examined using receiver operating characteristic analyses and calibration assessments. Across all three image types—T2WI, diffusion-weighted imaging, and ADC maps—patients presenting with excess syndromes showed significantly higher radiomic scores than those with deficiency syndromes. The T2WI, diffusion-weighted, and ADC models achieved areas under the ROC curve of 0.824, 0.824, and 0.847 in the training set, and 0.759, 0.750, and 0.809 in the validation set. Among these, the ADC-based model provided the strongest discriminatory capability, reaching accuracies of 0.788 in training and 0.778 in validation. Calibration results indicated good alignment between predicted radiomic outputs and actual TCM syndrome categories. Radiomics derived from MR imaging offers a feasible, non-invasive strategy for differentiating TCM deficiency versus excess syndromes in PCa, with ADC-related features demonstrating the highest diagnostic value.

Keywords: Prostate cancer, TCM syndrome, Magnetic resonance imaging, Radiomics

How to Cite This Article: Mansour K, Haddad O, Saleh R. Radiomic Signatures from Multiparametric MRI to Distinguish TCM Deficiency and Excess Syndromes in Prostate Cancer. Interdiscip Res Med Sci Spec. 2023;3(2):128-38. https://doi.org/10.51847/7QuTDSIz3Q

Introduction

Prostate cancer (PCa) is the second most frequently diagnosed malignancy among men globally [1]. Although its incidence in China remains lower than that reported in Western countries, both the occurrence and mortality of PCa have risen markedly in recent years [2]. Traditional Chinese Medicine (TCM) continues to play a significant role in PCa management, particularly for patients with advanced disease. In TCM, syndromes represent comprehensive summaries of pathological mechanisms, disease severity, and expected progression at specific clinical stages [3, 4]. Because syndrome differentiation relies heavily on the clinical experience of individual practitioners, a wide range of syndrome patterns has emerged in the context of PCa [5, 6]. A review by Si *et al.,* which examined 76 publications on TCM-related diagnosis and treatment of PCa from 1979 to 2014, identified 31 core TCM syndromes and as many as 254 variations [5]. The absence of a standardized framework for TCM syndrome differentiation in PCa has therefore posed challenges to systematic development in this field. Integrating objective, quantifiable indicators derived from modern medical technologies and artificial intelligence may help strengthen and modernize syndrome classification in PCa [7].

Magnetic resonance imaging (MRI) is broadly considered the imaging modality of choice for evaluating prostate disorders due to its superior soft-tissue contrast, high spatial resolution, and combined functional and anatomical

data. MRI plays a crucial role in the detection, localization, targeted biopsy, staging, risk stratification, and surveillance of PCa [8]. Among MRI sequences, T2-weighted imaging (T2WI), diffusion-weighted imaging (DWI), and corresponding apparent diffusion coefficient (ADC) maps are central to the assessment and diagnosis of PCa [9, 10].

Radiomics offers a method for extracting large volumes of quantitative, high-dimensional data from routine imaging, allowing such data to be transformed into analyzable biomarkers [11]. Recent work suggests that MRI-based radiomics can enhance PCa diagnosis [12, 13]. For example, Min *et al*. reported that a multiparametric MRI radiomics model achieved area-under-the-curve values of 0.872 and 0.823 for detecting PCa with Gleason score ≥3 + 4 in training and test cohorts, respectively [12]. Despite these advances, the potential of radiomics to predict TCM syndromes in PCa has not been examined. According to the traditional "eight principles," the opposing concepts of yin and yang—expressed clinically as deficiency and excess—capture the essence of most TCM syndrome categories [14, 15]. This theoretical framework simplifies the large variety of PCa-related TCM syndromes into two fundamental groups, making it feasible to explore syndrome classification through modern imaging analytics.

Therefore, the present study aimed to investigate whether MRI-derived radiomic signatures can differentiate between TCM excess and deficiency syndromes in patients with PCa.

Materials and Methods

Patient population

This retrospective investigation received approval from the local institutional ethics committees of both participating hospitals (Approval No: 2022KY051). Because of its retrospective design, the requirement for written informed consent was waived. Patients were recruited from two institutions: Hangzhou TCM Hospital Affiliated with Zhejiang Chinese Medical University (Center 1) and the First Affiliated Hospital of Zhejiang Chinese Medical University (Center 2). Syndrome differentiation was carried out according to the criteria outlined in *TCM Oncology* [15]. Cases categorized as spleen–kidney deficiency, dual deficiency of qi and yin, or qi–blood deficiency were assigned to the TCM deficiency group, whereas damp-heat accumulation, phlegm-blood stasis, and qi stagnation with blood stasis were designated as TCM excess syndromes. To ensure the consistency and reliability of syndrome classification, two associate chief physicians specializing in TCM independently evaluated each case.

Patients were eligible if: (1) PCa had been pathologically confirmed via radical prostatectomy or biopsy; (2) MRI examinations included T1WI, T2WI, and DWI acquired on a 3.0-T scanner; and (3) pathological assessment was completed within two months of the MRI study. Exclusion criteria included: (1) comorbidities capable of influencing TCM syndrome evaluation, such as acute respiratory infections, urinary tract infections, diabetes, or recent cardiovascular events; (2) any prior treatment for PCa before the MRI examination; and (3) inadequate image quality or tumor lesions measuring less than 5 mm on MRI. Of the 204 initially reviewed PCa patients, 83 were excluded based on these criteria, leaving 121 for final analysis. The cohort from Center 1 (n = 84) served as the training sample, while 37 patients from Center 2 formed the external validation set. Within the training group, 45 patients exhibited TCM excess syndromes and 39 were classified as deficiency syndromes; in the validation cohort, the numbers were 15 and 22, respectively. Clinical data extracted from electronic medical records included age and prostate-specific antigen (PSA) levels, with the PSA test performed within one month of the MRI scan.

MRI acquisition

All imaging was performed using either a GE Discovery MR750 or Siemens Magnetom Verio 3.0-T scanner, employing a pelvic phased-array coil. Prior to scanning, patients were instructed to maintain a moderately filled bladder. The imaging field encompassed the entire prostate and seminal vesicles. The MRI protocol consisted of axial T1-weighted imaging, axial and sagittal T2-weighted imaging, and axial diffusion-weighted imaging. DWI was obtained using b-values of 0–50 s/mm² and 800–1000 s/mm². Apparent diffusion coefficient maps were automatically generated on each scanner using a standard mono-exponential model.

Pathological evaluation

All patients underwent systematic transrectal ultrasound-guided biopsy, consisting of 10–12 cores, with additional cognitive-targeted sampling when MRI revealed suspicious lesions. The performing urologist localized biopsy

targets through cognitive fusion whenever appropriate. Each specimen was labeled individually according to its anatomical origin. Histopathological assessment was conducted following the International Society of Urological Pathology (ISUP) recommendations [16]. A radiologist with 22 years of experience in prostate MRI correlated MR findings with the reference standards—biopsy core locations and, when applicable, radical prostatectomy results—to identify the index lesion.

Lesion segmentation on MRI

Lesion delineation was performed using ITK-SNAP version 3.6.0 (www.itk-snap.org). A radiologist with seven years of dedicated experience in prostate MRI (Z.P.L.) manually outlined the regions of interest (ROIs), guided by corresponding pathological findings. Tumors were segmented in three dimensions to generate volumetric ROIs. In patients with multifocal disease, the index lesion—representing the site most reflective of tumor aggressiveness and biological behavior—was selected for analysis in accordance with established criteria [17, 18]. ROIs were drawn to encompass the tumor tissue as completely as possible while excluding adjacent non-neoplastic structures. Maximum tumor diameters were recorded on T2WI, and MRI-based T-staging was assigned using the National Comprehensive Cancer Network (NCCN) guidelines [19].

Radiomic feature extraction

The segmented ROIs from T2WI, DWI, and ADC images were imported into the Analysis Kit (AK, GE Healthcare, USA) for radiomic feature calculation. Each imaging sequence yielded 1,316 quantitative features, including first-order histogram metrics, shape descriptors, gray-level co-occurrence matrix (GLCM) features, gray-level run-length matrix (GLRLM) features, gray-level dependence matrix (GLDM) features, neighboring gray-tone difference matrix (NGTDM) features, gray-level size zone matrix (GLSZM) features, and wavelet-transformed variables.

Because the two participating centers used different scanner models and acquisition parameters, all images underwent preprocessing before feature extraction. This included resampling to an isotropic resolution of $1 \times 1 \times 1$ mm³ and normalizing gray levels to the 0–255 range to optimize comparability across datasets. Following extraction, all features were standardized using Z-score normalization ($(x-\mu)/\sigma$) where x represents the feature value, μ the mean across all patients for that feature, and σ the corresponding standard deviation. This step minimized the influence of scale differences and ensured consistent weighting within the machine-learning models.

Development of the radiomic signature

The radiomic signature was derived in two main stages. First, the minimum redundancy–maximum relevance (mRMR) method was used to remove features with high redundancy or limited correlation with the target classification. Second, the least absolute shrinkage and selection operator (LASSO) regression was applied to further refine the feature set by penalizing coefficients, setting noncontributory feature weights to zero, and selecting the most informative variables. The optimal regularization parameter (λ) was identified using 10-fold cross-validation to achieve the best predictive performance. The radiomic score (rad-score) for each patient was computed by summing the selected features weighted by their corresponding LASSO coefficients.

Model discrimination was assessed using receiver operating characteristic (ROC) analyses in both the training and validation datasets. Calibration curves were constructed to evaluate agreement between predicted probabilities and the actual classification of TCM deficiency and excess syndromes. Model goodness-of-fit was examined using the Hosmer–Lemeshow test; a P value greater than 0.05 indicated adequate concordance between the model predictions and observed outcomes [20]. The overall radiomics pipeline is illustrated in **Figure 1.**

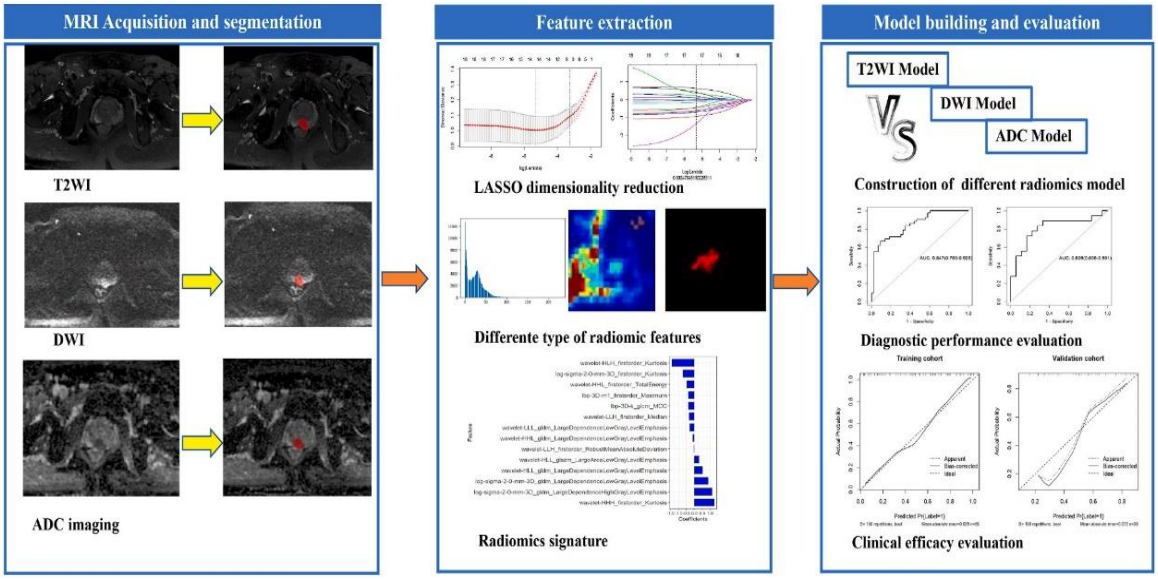

Figure 1. Workflow of the development of the radiomic model.

Statistical analysis

Statistical analyses were performed using R software (version 3.5.1) and SPSS version 25.0. For continuous variables, comparisons between groups were carried out using either the independent-samples *t*-test or the Mann–Whitney *U* test, depending on data distribution. Categorical variables were assessed with the chi-square test or Fisher's exact test when appropriate. Differences in the area under the ROC curves (AUCs) among the various predictive models were evaluated using the DeLong method. A two-tailed *P* value of less than 0.05 was considered indicative of statistical significance.

Results and Discussion

Patient demographic data

A total of 121 patients with PCa met the inclusion criteria, with 84 allocated to the training cohort and 37 to the validation cohort. **Table 1** summarizes the distribution of TCM syndromes as well as the clinical profiles for both groups. No statistically significant differences were observed between the TCM excess and deficiency syndrome groups with respect to age, total PSA, free PSA, lesion count, lesion location, maximal tumor diameter, MRI T-stage, or Gleason score in either cohort ($P > 0.05$), with the exception of lesion number in the training cohort, which showed a significant difference.

Table 1. Clinical characteristics of patients in the training and validation cohorts.

haracteristic	**Training Cohort**			**Validation Cohort**		
	Deficiency syndrome (n = 39)	**Excess syndrome** (n = 45)	**P**	**Deficiency syndrome** (n = 22)	**Excess syndrome** (n = 15)	**P**
Age (years)	73.56 ± 8.13	73.98 ± 8.93	0.826	72.32 ± 6.25	73.80 ± 7.83	0.527
Total PSA (ng/ml)	67.86 ± 173.01	66.55 ± 181.72	0.973	149.88 ± 323.96	84.45 ± 183.04	0.484
Free PSA (ng/ml)	5.54 ± 8.09	4.85 ± 8.14	0.696	8.45 ± 13.07	7.16 ± 11.24	0.757
TCM syndrome			**NA**			**NA**
Spleen-kidney deficiency syndrome	(n = 27)	-		(n = 13)	-	
Dampness-heat accumulation syndrome	-	(n = 22)		-	(n = 7)	

Deficiency syndrome of both qi and yin	(n = 7)	-		(n = 5)	-	
Phlegm-blood stasis syndrome	-	(n = 13)		-	(n = 5)	
Deficiency of Qi and Blood	(n = 5)	-		(n = 4)	-	
Qi stagnation and blood stasis syndrome	-	(n = 10)		-	(n = 3)	
Maximum diameter (mm)	20.90 ± 11.28	19.05 ± 10.77	0.446	24.94 ± 17.43	22.86 ± 11.95	0.691
MRI T-stage			**0.781**			**0.386**
T2	26 (66.7%)	33 (73.3%)		14 (63.64%)	7 (46.67%)	
T3	7 (17.9%)	7 (15.6%)		5 (22.73%)	5 (33.33%)	
T4	6 (15.4%)	5 (11.1%)		3 (13.64%)	3 (20.00%)	
Location			**0.932**			**0.591**
PZ	18 (46.2%)	19 (42.2%)		7 (31.82%)	5 (33.33%)	
TZ	11 (28.2%)	14 (31.1%)		13 (59.09%)	7 (46.67%)	
PZ and TZ	10 (25.6%)	12 (26.7%)		2 (9.09%)	3 (20.00%)	
Lesion number			**0.031***			**0.539**
1	29 (74.4%)	36 (80%)		14 (63.6%)	7 (46.7%)	
2	9 (23.1%)	3 (6.7%)		7 (31.8%)	6 (40%)	
3	1 (2.6%)	6 (13.3%)		1 (4.5%)	2 (13.4%)	
Gleason score			**0.535**			**0.127**
6	13 (33.3%)	12 (26.7%)		4 (18.2%)	3 (20.0%)	
7	7 (17.9%)	14 (31.1%)		12 (54.5%)	5 (33.3%)	
8	11 (28.2%)	14 (31.1%)		2 (9.1%)	6 (40.0%)	
9	7 (17.9%)	4 (8.9%)		4 (18.2%)	1 (6.7%)	
10	1 (2.6%)	1 (2.2%)		0 (0.0%)	0 (0.0%)	

fPSA: free prostate-specific antigen; n: numbers of patients; NA: not available; PZ: peripheral zone; TCM: traditional Chinese medicine; TPSA: total prostate-specific antigen; TZ: transition zone; *P: value < 0.05.

Construction of the radiomic signatures

To develop the radiomic models, the initial set of 1,316 features was first filtered and refined using the minimum redundancy–maximum relevance (mRMR) approach, followed by the LASSO regression to select the most informative variables. This process generated three independent models corresponding to T2WI, DWI, and ADC sequences. For the ADC-based model, 14 features were retained and combined to form the predictive signature **(Figures 2)**. The T2WI and DWI models were built from 17 features each, selected through the same workflow. Across both the training and validation cohorts, the resulting radiomic scores were consistently higher in tumors classified as TCM excess syndrome compared with deficiency syndrome, indicating a clear distinction between the two groups ($p < 0.05$, **Figures 3**).

ADC model

a)

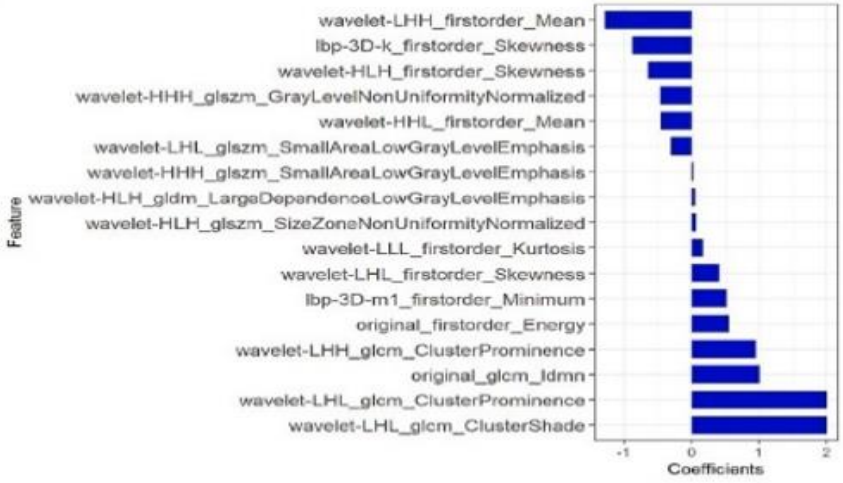

DWI model

b)

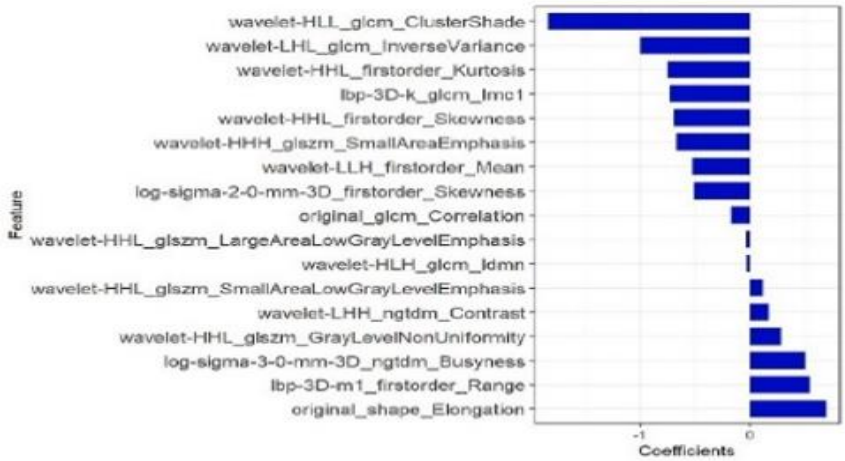

T2WI model

Figures 2. Overview of the features selected for constructing the radiomic models based on ADC, DWI, and T2WI sequences. Abbreviations: ADC, apparent diffusion coefficient; DWI, diffusion-weighted imaging; T2WI, T2-weighted imaging**.**

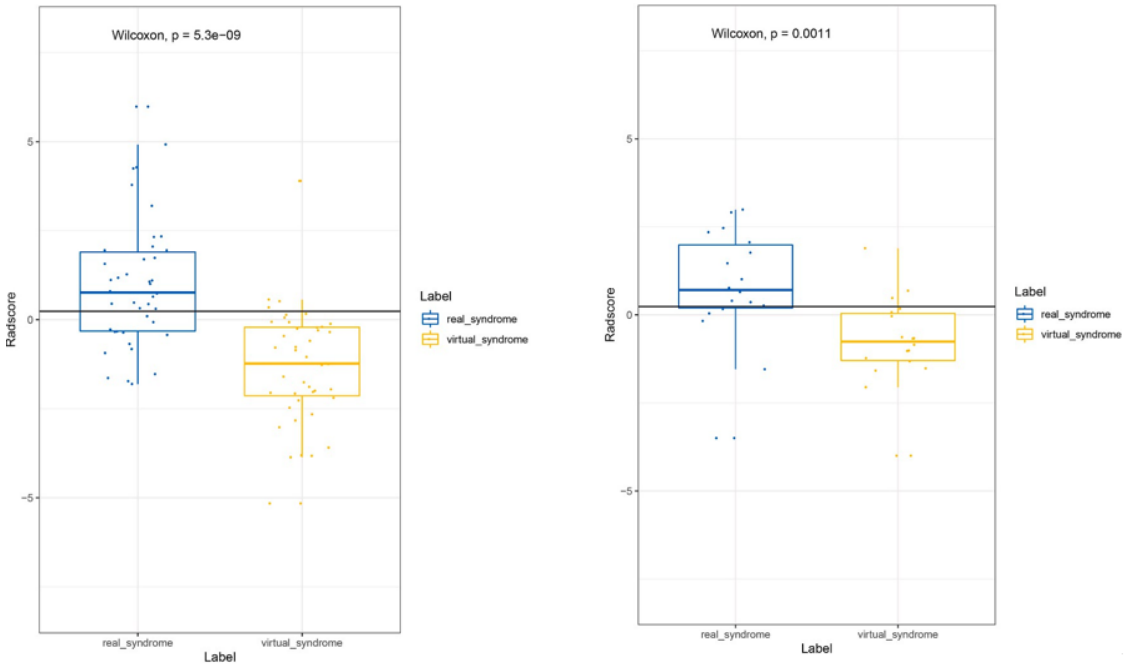

a) b)

Figures 3. Boxplots depicting ADC-based radiomic scores in patients with TCM deficiency versus excess syndromes across both training and validation cohorts. Significant differences are evident between the groups.

Abbreviations: Real_syndrome, excess syndrome; virtual_syndrome, deficiency syndrome.

Evaluation of model performance

The radiomic signatures derived from T2WI, DWI, and ADC sequences all demonstrated the ability to distinguish TCM deficiency from excess syndromes in prostate cancer. Notably, the ADC-based model exhibited the strongest predictive performance. In the training cohort, it achieved an accuracy of 78.8%, sensitivity of 70.8%, specificity of 90.7%, and an AUC of 0.847. Corresponding values in the validation cohort were 72.2% accuracy, 66.7% sensitivity, 83.3% specificity, and 0.809 AUC **(Table 2).**

Although the ADC model performed best, formal comparison using DeLong's test indicated that the differences in AUC among the T2WI, DWI, and ADC models were not statistically significant in either cohort ($P > 0.05$). Calibration analyses further demonstrated that predicted probabilities closely aligned with the observed classifications, suggesting the models reliably reflected the actual TCM syndrome distribution **(Figure 5).** Consistently, the Hosmer–Lemeshow goodness-of-fit test showed no evidence of poor model fit for any of the three radiomic signatures in either cohort ($P > 0.05$).

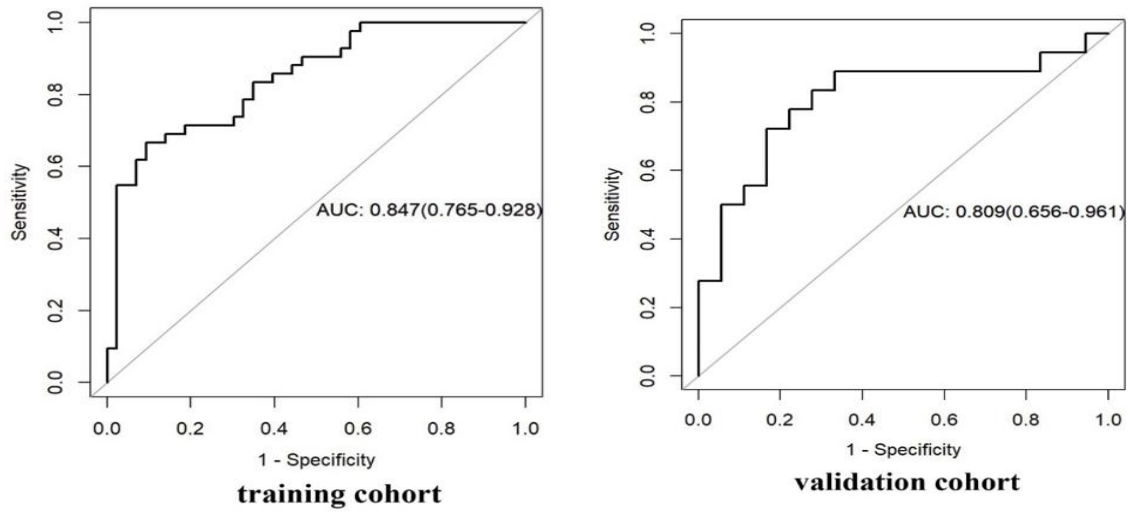

a) b)

Figure 4. Receiver operating characteristic (ROC) curves for the ADC-based radiomic model in distinguishing PCa patients with TCM excess syndrome from those with deficiency syndrome in both training and validation cohorts. Abbreviations: AUC, area under the ROC curve.

Table 2. Predictive performance of the radiomic model in the training and validation cohorts.

Model	Cohort	AUC (95% CI)	Sensitivity	Specificity	Accuracy	PPV	NPV
T2WI-based model	Training cohort	0.824 (0.730–0.914)	0.721	0.833	0.776	0.816	0.745
	Validation cohort	0.759 (0.603–0.916)	0.444	0.944	0.694	0.889	0.630
DWI-based model	Training cohort	0.824 (0.732–0.915)	0.884	0.690	0.788	0.745	0.853
	Validation cohort	0.750 (0.578–0.922)	0.944	0.611	0.778	0.708	0.917
ADC-based model	Training cohort	0.847 (0.765–0.928)	0.907	0.667	0.788	0.736	0.875
	Validation cohort	0.809 (0.656–0.961)	0.722	0.833	0.778	0.813	0.750

AUC: area under the receiver operating characteristic curve; 95 % CI: 95 % confidence interval; NPV: negative predictive value; PPV: positive predictive value.

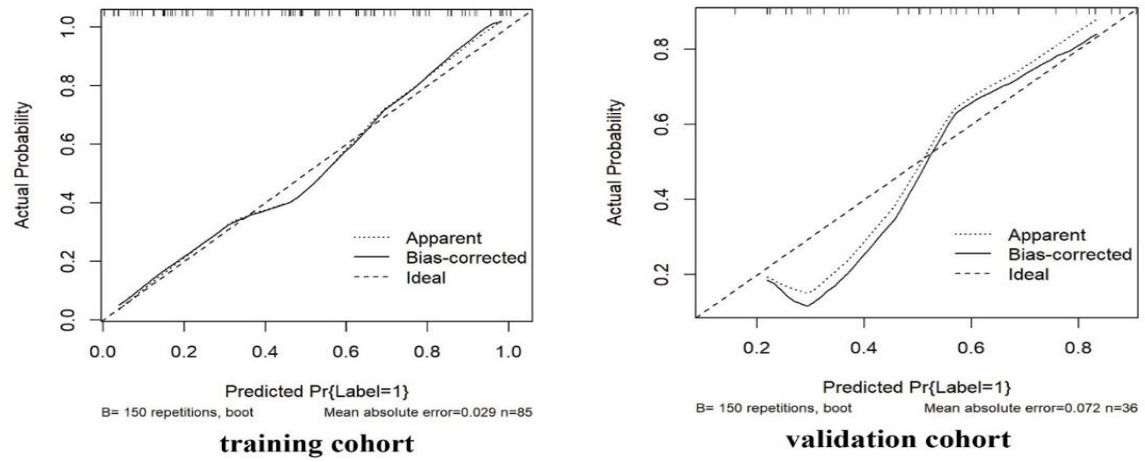

a) b)

Figure 5. Calibration curves for the ADC-based radiomic model predicting TCM excess syndrome in PCa patients across both training and validation cohorts. These curves illustrate the agreement between predicted probabilities and observed outcomes. Abbreviations: Pr, predicted probability.

In this study, we developed and externally validated MRI-based radiomic models aimed at distinguishing PCa patients with TCM excess syndrome from those with deficiency syndrome. Across both cohorts, the radiomic signatures derived from T2WI, DWI, and ADC sequences showed strong classification performance. By providing quantitative information directly from imaging data, radiomics offers a more objective approach to TCM syndrome differentiation, complementing traditional assessments based on clinical presentation, tongue examination, and pulse evaluation. These findings suggest that MRI radiomics could serve as a non-invasive, computational tool for assessing TCM deficiency and excess syndromes in PCa patients.

The lack of standardized criteria for TCM syndrome classification has hindered its broader clinical adoption. Integrating modern diagnostic techniques and objective biomarkers may help establish more reproducible differentiation strategies [7]. Prior studies have demonstrated the biological basis of TCM syndromes in cancer. For instance, single-cell RNA sequencing revealed that colorectal cancer patients with distinct TCM syndromes—excess, deficiency, or mixed deficiency-excess—showed significant differences in immune cell subset distributions [21]. Similarly, laboratory parameters such as total bilirubin, hemoglobin, uric acid, and hematocrit were reported to correlate with TCM syndromes in colorectal cancer patients [22]. However, few studies have explored the use of radiomics to predict TCM syndromes in PCa.

Our results demonstrate that radiomic signatures from T2WI, DWI, and ADC images can successfully differentiate excess from deficiency syndromes in PCa. These models extract quantitative features from MR images, enabling computational and reproducible evaluation of TCM syndromes, which represents a step toward more objective syndrome assessment.

Among the three imaging modalities, the ADC-based model achieved superior discrimination. This likely reflects the underlying principles of DWI and ADC imaging, which provide insights into tumor cellularity and tissue microstructure [23]. DWI assesses the microscopic motion of water molecules, offering a non-invasive measure of tissue density and cellular organization, and is considered particularly valuable for evaluating the peripheral zone of the prostate [9, 10]. ADC values, derived from DWI, have been recognized as reliable quantitative markers of tumor aggressiveness in PCa [24].

Moreover, the relationship between TCM syndromes and PCa pathology may explain these findings. In early-stage PCa, excess-related syndromes such as qi stagnation and blood stasis are more common, whereas deficiency syndromes, including spleen and kidney deficiency, tend to predominate in advanced disease [25]. The ADC model may therefore capture imaging features that correlate with these pathological and functional changes, enhancing its ability to differentiate TCM syndromes in PCa.

Most of the features selected for inclusion in the T2WI, DWI, and ADC radiomic models were derived from wavelet transformations. This suggests a potential link between wavelet-based imaging features and TCM syndrome classification in PCa. Wavelet transformation is a multiscale image analysis technique that decomposes three-dimensional imaging data into different frequency components along multiple axes [26]. This finding aligns with prior studies in radiomics. For example, a support vector machine-based radiomics study investigating lymph node status in intrahepatic cholangiocarcinoma relied exclusively on five wavelet-derived features to build the predictive model [27]. Such evidence indicates that wavelet features serve as robust imaging biomarkers, reflecting tumor pathology and aggressiveness.

In the present study, tumor segmentation was performed manually by a single experienced radiologist to ensure accuracy and consistency. Pathology reports were used as the reference standard during ROI delineation. While manual segmentation is time-intensive, automated approaches for prostate cancer remain challenging. Previous work by Young *et al*. demonstrated that deep learning algorithms can match the performance of less experienced radiologists in lesion detection and PI-RADS scoring [28]. Nonetheless, manual delineation by an expert remains a reliable method for achieving precise and reproducible tumor contours in the context of radiomics studies.

This study has several limitations. First, its retrospective design and relatively small sample size limit the generalizability of the findings. Prospective studies with larger and more diverse cohorts are necessary to validate the predictive capability of MR-based radiomics for TCM syndrome classification in PCa. Second, lesions smaller than 5 mm on MRI were excluded due to challenges in accurate segmentation, which may introduce selection bias. Despite these constraints, the methodological approach employed here provides strong internal validation of the primary findings.

Conclusion

MR imaging-derived radiomic signatures offer a non-invasive, quantitative approach for distinguishing TCM deficiency from excess syndromes in PCa, with the ADC-based model demonstrating superior diagnostic performance. Future studies with larger, prospective cohorts are warranted to confirm these preliminary results. Ultimately, radiomics may provide an objective, reproducible framework to support TCM syndrome classification in clinical management of prostate cancer.

Acknowledgments: None

Conflict of Interest: The authors declare the following financial interests/personal relationships which may be considered as potential competing interests:Yongsheng Zhang reports article publishing charges was provided by the Chinese Medical Health Science and Technology Project of Zhejiang Provincial Health Commission. Zhiping Li reports article publishing charges was provided by the Medical Health Science and Technology Project of Zhejiang Provincial Health Commission. Feng Cui reports article publishing charges was provided by Hangzhou Social Development Research Project. Yuguo Wei reports a relationship with Global Medical Service, GE Healthcare that includes: employment. If there are other authors, they declare that they have no known competing financial interests or personal relationships that could have appeared to influence the work reported in this paper.

Financial Support: This work was partly supported by the Chinese Medical Health Science and Technology Project of Zhejiang Provincial Health Commission (2022ZA102), the Medical Health Science and Technology Project of Zhejiang Provincial Health Commission（2022KY996) and Hangzhou Social Development Research Project（202204B07).

Ethics Statement: None

References

1. F. Bray, J. Ferlay, I. Soerjomataram, R.L. Siegel, L.A. Torre, A. Jemal, Global cancer statistics 2018: GLOBOCAN estimates of incidence and mortality worldwide for 36 cancers in 185 countries, Cancer J Clin 68 (6) (2018) 394–424.
2. Z.T. Fu, X.L. Guo, S.W. Zhang, R.S. Zheng, H.M. Zeng, Chen Ru. Statistical analysis of incidence and mortality of prostate cancer in China, 2015, Chin. J. Oncol. 42 (9) (2020) 718–722.
3. A. Lu, M. Jiang, C. Zhang, K. Chan, An integrative approach of linking traditional Chinese medicine pattern classification and biomedicine diagnosis, J. Ethnopharmacol. 141 (2) (2012) 549–556.
4. X.Q. Liu, R.S. Zhang, X.Z. Zhou, H. Zhou, Y.Y. He, S. Han, et al., Analysis of Chinese medical syndrome features of ischemic stroke based on similarity of symptoms subgroup, Chin. J. Integr. Med. (2022), 35723812.
5. F.C. Si, C.F. Du, Analysis of TCM syndromes and prescriptions rules in prostatic carcinoma, Chinese Journal of Traditional Chinese Medicine (Chin) 30 (2) (2015) 581–585.
6. Y.J. Jia, J. Chen, X.J. Li, X.Q. Wang, W.T. Xu, Literature analysis on TCM syndrome of prostate cancer, Liaoning Journal of Traditional Chinese Medicine (Chin) 41 (9) (2014) 1850–1852.
7. N. Li, J. Yu, X. Mao, Y. Zhao, L. Huang, The research and development thinking on the status of artificial intelligence in traditional Chinese medicine, Evid Based Complement Alternat Med 2022 (2022), 7644524.
8. J.E. Thompson, P.J. van Leeuwen, D. Moses, R. Shnier, P. Brenner, W. Delprado, et al., The diagnostic performance of multiparametric magnetic resonance imaging to detect significant prostate cancer, J. Urol. 195 (5) (2016) 1428–1435.
9. J.C. Weinreb, J.O. Barentsz, P.L. Choyke, F. Cornud, M.A. Haider, K.J. Macura, et al., PI-RADS prostate imaging reporting and data system: 2015, version 2, Eur. Urol. 69 (1) (2016) 16–40.
10. B. Turkbey, A.B. Rosenkrantz, M.A. Haider, A.R. Padhani, G. Villeirs, K.J. Macura, et al., Prostate imaging reporting and data system version 2.1: 2019 update of prostate imaging reporting and data system version 2, Eur. Urol. 76 (3) (2019) 340–351.
11. S.S. Yip, H.J. Aerts, Applications and limitations of radiomics, Phys. Med. Biol. 61 (13) (2016) R150–R166.
12. X. Min, M. Li, D. Dong, Z. Feng, P. Zhang, Z. Ke, et al., Multi-parametric MRIbased radiomics signature for discriminating between clinically significant and insignificant prostate cancer: cross-validation of a machine learning method, Eur. J. Radiol. 115 (2019) 16–21.

13. Y. Zhang, W. Chen, X. Yue, J. Shen, C. Gao, P. Pang, et al., Development of a novel, multi-parametric, MRI-based Radiomic nomogram for differentiating between clinically significant and insignificant prostate cancer, Front. Oncol. 10 (2020) 888.
14. F. Cheung, TCM: made in China, Nature 480 (7378) (2011) S82–S83.
15. Daihan Zhou, Oncology of Traditional Chinese Medicine, first ed., China Press of Traditional Chinese Medicine (Chin), Beijing, 2011, pp. 308–315.
16. G.J.L.H. van Leenders, T.H. van der Kwast, D.J. Grignon, A.J. Evans, G. Kristiansen, C.F. Kweldam, et al., The 2019 international society of urological pathology (ISUP) consensus conference on grading of prostatic carcinoma, Am. J. Surg. Pathol. 44 (8) (2020) e87–e99.
17. E. Baco, O. Ukimura, E. Rud, L. Vlatkovic, A. Svindland, M. Aron, et al., Magnetic resonance imaging–transectal ultrasound image-fusion biopsies accurately characterize the index tumor: correlation with step-sectioned radical prostatectomy specimens in 135 patients, Eur. Urol. 67 (4) (2015) 787–794.
18. J.D. Le, N. Tan, E. Shkolyar, D.Y. Lu, L. Kwan, L.S. Marks, et al., Multifocality and prostate cancer detection by multiparametric magnetic resonance imaging: correlation with whole-mount histopathology, Eur. Urol. 67 (3) (2015) 569–576.
19. P.H. Carroll, J.L. Mohler, NCCN Guidelines updates: prostate cancer and prostate cancer early detection, J Natl Compr Canc Netw 16 (5S) (2018) 620–623.
20. P. Paul, M.L. Pennell, S. Lemeshow, Standardizing the power of the Hosmer-Lemeshow goodness of fit test in large data sets, Stat. Med. 32 (1) (2013) 67–80.
21. Y. Lu, C. Zhou, M. Zhu, Z. Fu, Y. Shi, M. Li, et al., Traditional Chinese medicine syndromes classification associates with tumor cell and microenvironment heterogeneity in colorectal cancer: a single cell RNA sequencing analysis, Chin. Med. 16 (1) (2021) 133.
22. Y.N. Wang, M. Zou, D. Wang, Z.K. Zhang, L.P. Qu, J. Xu, et al., An exploratory study on TCM syndrome differentiation in preoperative patients with colorectal cancer assisted by laboratory indicators, 14, Heliyon 8 (8) (2022), e10207.
23. A. Chatterjee, G. Watson, E. Myint, P. Sved, M. McEntee, R. Bourne, Changes in epithelium, stroma, and lumen space correlate more strongly with gleason pattern and are stronger predictors of prostate ADC changes than cellularity metrics, Radiology 277 (2015) 751–762.
24. A. Hoang Dinh, C. Melodelima, R. Souchon, J. Lehaire, F. Bratan, F. M`egeLechevallier, et al., Quantitative analysis of prostate multiparametric MR images for detection of aggressive prostate cancer in the peripheral zone: a multiple imager study, Radiology 280 (2016) 117–127.
25. Z.Q. Chen, S.S. Wang, Z.G. Bai, Z.H. Wang, L.G. Lv, C.M. Gu, et al., Staging based strategies and practice for prostate cancer, Chinese Journal of Integrated Traditional and Western Medicine (Chin) 36 (6) (2016) 749–752.
26. A. Kassner, R. Thornhill, Texture analysis: a review of neurologic MR imaging applications, AJNR Am J Neuroradiol 31 (5) (2010) 809–816.
27. L. Xu, P. Yang, W. Liang, W. Liu, W. Wang, C. Luo, et al., A radiomics approach based on support vector machine using MR images for preoperative lymph node status evaluation in intrahepatic cholangiocarcinoma, Theranostics 9 (18) (2019) 5374–5385.
28. S.Y. Youn, M.H. Choi, D.H. Kim, Y.J. Lee, H. Huisman, E. Johnson, et al., Detection and PI-RADS classification of focal lesions in prostate MRI: performance comparison between a deep learning-based algorithm (DLA) and radiologists with various levels of experience, Eur. J. Radiol. 142 (2021), 109894.